

Design, integration, and field evaluation of a robotic apple harvester

Abhisesh Silwal^{1*} | Joseph R. Davidson^{2*} | Manoj Karkee³ | Changki Mo⁴ | Qin Zhang⁵ | Karen Lewis⁶

¹Biological Systems Engineering Department, Center for Precision and Automated Agricultural Systems, Washington State University, USA

²School of Mechanical and Materials Engineering, Washington State University, USA

³Biological Systems Engineering Department, Center for Precision and Automated Agricultural Systems, Washington State University, USA

⁴School of Mechanical and Materials Engineering, Washington State University, USA

⁵Biological Systems Engineering Department, Center for Precision and Automated Agricultural Systems, Washington State University, USA

⁶Extension, Center for Precision and Automated Agricultural Systems, Washington State University, USA

Correspondence
Manoj Karkee, 24106 N Bunn Rd, CPAAS, Prosser, WA 99350, USA.

Email: manoj.karkee@wsu.edu

*These authors contributed equally to this work

Abstract

Every apple destined for the fresh market is picked by the human hand. Despite extensive research over the past four decades, there are no mechanical apple harvesters for the fresh market commercially available, which is a significant concern because of increasing uncertainty about the availability of manual labor and rising production costs. The highly unstructured orchard environment has been a major challenge to the development of commercially viable robotic harvesting systems. This paper reports the design and field evaluation of a robotic apple harvester. The approach adopted was to use a low-cost system to assess required sensing, planning, and manipulation functionality in a modern orchard system with a planar canopy. The system was tested in a commercial apple orchard in Washington State. Workspace modifications and performance criteria are thoroughly defined and reported to help evaluate the approach and guide future enhancements. The machine vision system was accurate and had an average localization time of 1.5 s per fruit. The seven degree of freedom harvesting system successfully picked 127 of the 150 fruit attempted for an overall success rate of 84% with an average picking time of 6.0 s per fruit. Future work will include integration of additional sensing and obstacle detection for improved system robustness.

KEY WORDS

apple, cycle time, machine vision, manipulator, robotic harvesting

1 | INTRODUCTION

During the twentieth century, technological advances in agricultural mechanization fundamentally altered the structure of modern agriculture. The tractor and combine harvester have all but eliminated the need for manual labor during the production of bulk commodity crops like corn and wheat. Despite this rapid progress in agricultural automation, the production of high-value specialty crops, which the U.S. Department of Agriculture (USDA) defines as fruits and vegetables, tree nuts, dried fruits, horticulture, and nursery crops,¹ is still largely dependent on manual labor. For example, in the U.S. Pacific Northwest, a large, seasonal labor force is required for the production of fresh market apples. Activities requiring significant manual labor include pruning, thinning, and harvesting. During 2013, seasonal employment in Washington State for apple pruning and thinning peaked at 8,508 and 17,349 workers, respectively. However, the most labor-intensive task in tree fruit crop production is harvesting, which required 36,425 seasonal agricultural workers during September, the peak harvesting month.² Local growers report that harvesting labor

accounts for approximately a third of their annual variable costs—as much as pruning and thinning combined.³ Harvesting is also a time-sensitive operation where variable weather patterns create uncertainty during employment planning. For example, the threat of an early fall frost can cause a short-term surge in the demand for apple pickers.

Like many agricultural sectors around the world, the fresh market apple industry is struggling to cope with rising labor costs and increasing uncertainty surrounding the future availability of farm labor.^{4,5} In the United States, the majority of the seasonal labor force is supplied by migrant Latino populations. A recent study by the Pew Research Center found that over the past five years net migration from Mexico to the United States has been negative.⁶ All fresh market apples are picked by hand using a ladder and bag. Picking fresh market apples is semi-skilled work that is both physically strenuous and highly repetitive. Apple picking exposes workers to fall hazards as well as ergonomic injuries through heavy lifting and repetitive hand actions.⁷ There are harvest/labor assist systems commercially available, like mechanical platforms that raise workers to the fruit and raise the fruit bin to the workers, but adoption is not widespread in Washington or in orchards

in the Eastern region of the United States.⁸ A recent survey of 316 Washington apple operations⁹ found that only eleven percent of growers used mechanical platforms. Incompatibility between the platforms and the existing orchard architecture and tree structure was cited as the most significant impediment to their use. A study of platform use during pear harvesting in California orchards¹⁰ also cited the issue of orchard–platform compatibility as a significant problem. So, in addition to the risks associated with labor availability and rising costs, worker safety concerns also motivate increased interest and research in harvest mechanization in fresh market apple production. The lack of mechanical harvesting for fresh market apples is a critical problem that threatens the U.S. tree fruit industry's long-term sustainability.

To reduce harvesting costs and dependence on seasonal labor, researchers have proposed two different approaches for total mechanization of tree fruit harvesting. The first method is bulk harvesting with shake-and-catch systems^{11–14} that apply vibration to the trunk or branch of the tree to separate the fruit. The shake-and-catch approach has generally resulted in damage levels that are unacceptable for fresh market fruit. Minimizing damage caused by fruit to fruit/branch¹⁵ contact as well as damage resulting from fruit impact with the catching surface¹⁶ are subjects of active research. The second method is selective fruit harvesting with robotics technology. Scientists and engineers started to actively work on research and development of fruit-picking robots in the 1980s.^{17,18} The typical approach adopted has been to integrate a machine vision system with a manipulator and end-effector in order to selectively pick individual ripe fruit.¹⁹ Despite numerous attempts over the past three decades to transfer industrial robotics technology directly to this field-based, biologically driven environment, there are no known commercial implementations of robotic harvesting systems for specialty crop agriculture.¹⁹ As will be more thoroughly discussed in Section 2, limitations of previous robotic platforms include insufficiently robust fruit detection and manipulation as well as high overall harvesting cycle times.

Considering the industry need and extensive resources devoted to robotic harvesting research and development, the question becomes why have robotic tree fruit harvesting systems not yielded performance levels required for commercial viability? Most prominently, the unstructured orchard environment has proven very challenging. Some of these challenges include variable outdoor environmental conditions, complex tree structures, fruit clusters and occlusion, inconsistency in fruit shape and size, and fruit sensitivity to damage. Over the past thirty years, there have been considerable advances in horticultural practices. Modern orchard systems with planar canopies have led to improved quality, yield, and labor efficiencies.⁸ Modern planar systems allow for increased uniformity in fruit size, color and maturity within an individual tree and across a single varietal block of trees. This paper presents a bottom-up hierarchical approach to assess the required functionality of a robotic harvesting system in today's modern apple orchards with fruiting wall architectures. The growing region considered is Eastern Washington, the largest producer of fresh market apples in the United States. The proposed system uses vision sensors to detect and localize apples at the beginning of a harvesting cycle. After fruit localization, the system proceeds with apple picking using

no additional sensory input. Unlike the apple picking method used by professional pickers, the robotic harvesting method described in this paper is not selective to fruit orientation and stem location, hence, the system is considered "undersensed." The goal was to assess baseline harvesting performance using a relatively low-cost robotic system. The remainder of this paper is organized as follows: Sections 2 and 3 discuss prior work in the field and how lessons learned from previous research guided certain design selections. The robotic harvesting system's working environment is described in Section 4. Sections 5,6, and 7 present the integrated system, vision system, and mechanical design. A key step in the design process was the development of a manipulation system robust to perception error acquired during fruit localization. As will be described in Section 7, the integrated robotic picking method is partly based on a previous study²⁰ of the hand picking process. Section 8 reports the results and observations obtained from field testing of the robotic system in a commercial orchard. In their recent review of harvesting robots, Bac et al.¹⁹ noted that the absence of and inconsistencies in reporting criteria used in the research community made it difficult to assess and compare the performance of the state-of-the-art in the field. To address this observation, this work measures system performance with the use of thoroughly defined reporting criteria. A discussion of additional functionality required for improved system robustness is included at the end of the paper.

2 | PRIOR WORK

Robotic harvesting is a complex and challenging problem. A significant bottleneck to commercial development is the extensive variability that exists in the unstructured agricultural environment. Because the challenges of robotic harvesting have been well-documented in several reviews of complete systems,^{19,21–23} the literature review included here is brief and tailored to a discussion of issues that have limited the performance of robotic apple harvesters.

2.1 | Fruit identification

An autonomous robotic harvesting system needs to visually sense the apples prior to picking. It is an essential component of the system that provides the position of identified fruit as input to the manipulation system. Over the past several decades, researchers have developed and implemented various machine vision-based methods for fruit identification. With increasing sensing and computational capability, a large number of fruit-identification work has been reported in the last decade. Color is the most commonly used feature to segregate fruit from vegetation and background.^{24,25} Color-based segmentation for detection of fruits with distinct colors, including apples, mangoes, pineapples, tomatoes, and citrus, has been investigated by Qiang et al.,²⁶ Hannan and Burks (2007), Slaughter and Harrell,²⁷ Bin et al.,²⁸ Silwal et al.,²⁹ and Silwal et al.³⁰ In addition to the color feature, researchers have also used global mixtures of Gaussians with texture-based segmentation,^{31,32} Circular Hough Transform,³³ Blob Analysis,²⁹ region growing,³⁴ and geometric properties^{33,35,36} for fruit

identification. In general, these studies have achieved fruit identification accuracy ranging from 80% to 95% and have reported variable lighting conditions, clustering, and occlusion as the most significant challenges for accurate fruit identification in the orchard environment.³²⁻³⁹

Image segmentation, a primary step in fruit identification, is greatly affected by variable lighting altering color and texture properties essential for fruit detection.^{25,32,36} For these reasons, segmentation has often been a major source of error in vision systems.^{25,26,29,31} To minimize the effects of direct sunlight, researchers have designed systems to acquire images at sunset³⁶ and night.^{40,41} However, such an approach limits fruit picking opportunities during the time-sensitive harvest window. Unlike these approaches, recent work by Barnea et al.,²⁵ combined three-dimensional surface normal, plane-reflective symmetry, and plane highlights from elliptical surfaces to detect sweet peppers independent of their color. Implementation of machine learning tools for pixel classification and fruit identification has also been noticed in recent years. Artificial Neural Networks^{42,43} and Support Vector Machines^{34,39,44,45} are the most popular choices in the literature for robotic apple harvesting. The most promising results for fruit identification in outdoor environments using such techniques was reported in the work by Hung, Underwood, Nieto, and Sukkarieh.⁴⁶ In their lexicon, multi-class image segmentation was achieved using a generalized multi-scale feature learning approach. Results using a large dataset (8000 color images) taken under natural lighting conditions showed a classification accuracy of 93% between apple and non-apple classes. Fruit identification accuracy was presented as an R^2 value (0.81) between the algorithm count and ground truth of apples. Currently, this approach as designed for fruit yield estimation is computationally expensive (30 s per frame) and doesn't address additional needs for robotic harvesting such as fruit localization, prioritization, and selective harvesting strategies. Our earlier work,²⁹ which was tested in a commercial orchard environment in both day and night conditions (see Section 6), used a supportive structure with artificial lights to control variation in lighting and achieved similar accuracy with a relatively simple segmentation and identification approach.

2.2 | Manipulation

The performance of an early apple harvesting robot¹⁷ was limited by orchard architecture. The system used a four degree-of-freedom (DOF) manipulator with a vacuum end-effector. While overall cycle time was relatively low, harvesting efficiency was limited to 70% primarily due to crossover branches in hedgerow plantings limiting direct line of vision and manipulation to the fruit. Another problem encountered was fruit dropping from clusters. Researchers have repeatedly cited end-effector robustness as an unresolved issue in more recent work. A group in Belgium⁴⁷ used a seven DOF system with a vacuum activated, flexible gripper and documented 30% stem pulls during field trials in a Jonagold orchard. Overall harvesting cycle time was 8–10 s/fruit and, similar to observations from Grand d'Esnon et al.,¹⁷ clustered fruit were also problematic. The apple harvesting robot tested in Japan⁴⁸ had three DOF and used an end-effector that removed fruit

by pinching and rotating the stem. While contact with only the stem was considered advantageous because it minimized the likelihood of fruit bruising, the system was constrained to a horizontal approach and had difficulty detaching apples with short stems. An apple harvesting robot recently developed in China⁴⁹ used an electric blade to cut the stem after it was gripped by a spoon-shaped end-effector. The reported average harvesting time for this system, which used an eye-in-hand sensor setup for fruit localization, was 15.4 s/apple. A recommendation for future work was a redesigned end-effector more robust to grasping fruit with variable shape and size.

It is interesting to note that robotic harvesting systems implementing fruit removal methods that gripped the stem⁴⁸ or cut the stem⁴⁹ were used in Fuji orchards. As sensory detection of the stem is not described in the literature, it is believed that the implemented fruit detachment methods assumed all stems were vertical and accessible. Of the five apple varieties considered in our previous work,²⁰ Fuijis had the longest stems. Because both apple orientation and accessibility of the stem-abscission joint above the stem cavity of the fruit are highly variable, it is unclear whether manipulation methods assuming a vertical and accessible stem are robust for all apple varieties.

In their recent literature review, Bac et al.¹⁹ noted that performance improvements over the last thirty years have been partially constrained by an absence of reporting on test conditions, performance indicators, hardware systems, and software systems. This observation is valid for robotic apple harvesting research. For example, detailed descriptions of the orchard systems and test conditions used for field trials in the literature are lacking. Likewise, there is significant variability in the reported performance indicators. For example, the 7.1 s time reported by Bulanon and Kataoka⁴⁸ measures detachment time after the end-effector was pre-positioned on the stem. It is unknown how overall cycle time, which also includes reaching for and removal of the fruit, compares to other cycle times reported in the literature. To ensure that the community has a full understanding of the advantages and disadvantages of the proposed system, this paper provides thorough descriptions of the working environment, test conditions, hardware, and planning.

3 | SYSTEM REQUIREMENTS

The basic functional requirements of an apple harvesting robot include the following general tasks:

1. Identify fruit in the scene, localize each fruit in a 3-dimensional space, and prioritize apples for an optimal harvesting strategy. Additionally, fruit quality such as ripeness and minimal surface defects are also desired.
2. Detach the target fruit from the tree without bruising.
3. Guide the harvested fruit to a storage container.
4. Operable under both nighttime and natural daylight conditions as well as different weather conditions.
5. A system sufficiently robust such that it can be used for harvesting multiple apple varieties with different shapes, sizes, and color.

6. Compatible with different modern orchard designs, such as the V-trellis and vertical trellis architectures.
7. A relatively simple and cost-effective mechanical design that can be repaired in the field in the event of mechanical failure.

System design selections require a balance between speed, cost, and robustness. A detailed economics analysis of robotic apple harvesting is beyond the scope of this paper. While an economics assessment of harvest assist platforms has recently been completed,⁹ a similar assessment of robotics technology is needed to assist with the selection of specific design criteria and performance specifications. The fundamental goal of this research was to design a robotic system capable of high fruit detachment efficiency at relatively high speed with acceptable levels of fruit damage. Our strategy was to initially prioritize low-cost and speed in order to assess performance thresholds in best-case conditions where grower input was used to modify the crop environment in support of robotic harvesting. The adopted hierarchical approach uses the results from field trials to determine what additional functionality is required for future work. The general criteria adopted for the preliminary design was based on guidelines mentioned at the beginning of this section.

4 | CROP ENVIRONMENT AND WORKSPACE MODIFICATIONS

A commercial apple orchard ("Envy" variety) employing a modern, V-trellis fruiting wall architecture was selected for field studies during this research. The trees were trained in a formal architecture resulting in narrow planar tree canopies with branches secured along trellis wires. As shown in Figure 1, in this orchard system the fruit are distributed laterally along the branches in a fruit wall. Compared to traditional tree canopies where fruit distribution is three dimensional, this design presents fewer interfering obstacles from adjacent branches and enhances access. Industry trends are toward increased use of planar orchard systems in future plantings.⁵⁰ Field measurements showed an average fruit density of 19 apples per branch between two adjacent trees spaced approximately 142 cm apart. Average tree height was 366 cm. Table 1 provides the mean physical parameters of the orchard system and apple variety.

Previous work⁵¹ has shown that obstacle detection and collision-free motion planning for robotic harvesting is a challenging and computationally intense problem. Implementation of obstacle detection/avoidance has not been reported in prior robotic apple harvesting research. For the bottom-up assessment of functionality adopted

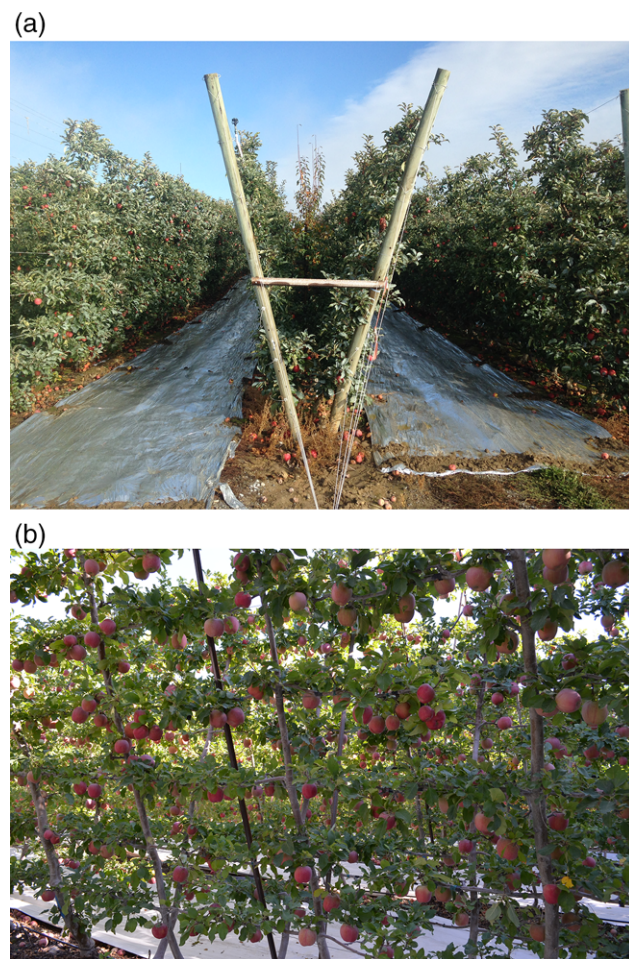


FIGURE 1 V-trellis orchard system used at a commercial apple orchard in Prosser, WA

for this research, obstacle detection algorithms are not used. This approach simplifies the harvesting task and reduces cycle time. However, not implementing obstacle detection requires workspace modifications to reduce the likelihood of unintended collisions and system damage. For a robotic harvester, problematic fruit are those adjacent to tree trunks and trellis wires (see Fig. 2). During numerous conversations with the authors, Washington State apple producers have expressed a willingness to thin fruit in a manner that would facilitate robotic harvesting; they have also indicated confidence that such modifications are possible without significant effects on total yield. This includes thinning a double cluster to a single fruit and removing fruit that are adjacent to wires, adjacent to trunks, and those behind the wire in a V-trellis system. Market dynamics, horticultural practices, and

TABLE 1 Mean physical parameters and standard deviations of the cultivation system and apple variety selected for field testing²⁰

Variety	Architecture	No. of wires	Trellis wire spacing (cm)	Tree spacing (cm)	Row width (cm)	Tree height (cm)	Fruit density (fruit per linear meter of branch)
Envy	V-Trellis	7	46 ± 1	142 ± 19	353 ± 3	366	19 ± 6
Major Axis (mm)		Minor Axis (mm)			Weight (gram)		Stem Length (mm)
76 ± 6		80 ± 4			255 ± 45		22 ± 4

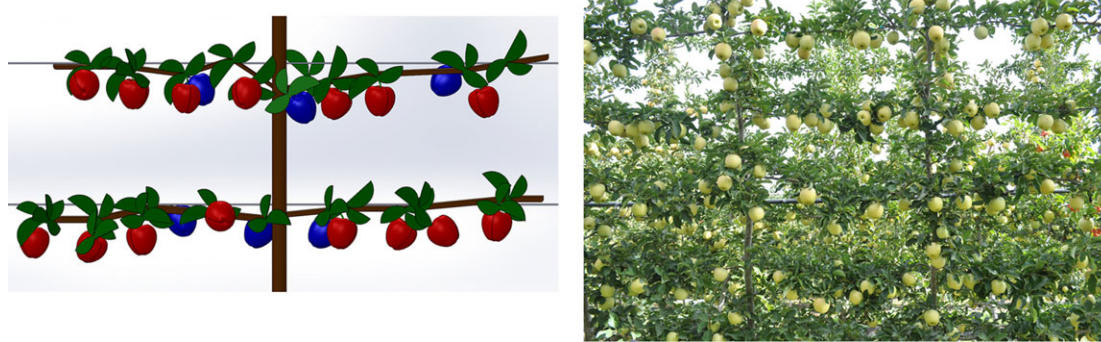


FIGURE 2 A graphic (left) (with an accompanying photo of representative fruit distribution (right)) depicting selective thinning of apples adjacent to obstacles. The blue fruits are those that would be removed prior to field testing

resource availability vary from region to region, so the ability of producers outside of Washington to make fruit placement modifications is unknown. Regardless, workspace modifications are described here so that readers can assess the applicability of test conditions and the robotic picking technique presented in this paper. After assessing fruit distribution, three categories of apples were removed prior to robotic harvesting. These categories included apples whose surface was within 1) 5 cm of a tree trunk, 2) 5 cm of a trellis wire, and 3) directly behind a trellis wire in relation to the harvesting system. The 5 cm threshold was a subjective criterion primarily determined by the open span of the end-effector, which was a function of apple size and standard deviation in fruit localization by the vision system. The average fruit density after thinning was eight to ten fruit per linear meter of trellis wire.

5 | SYSTEM OVERVIEW

Autonomous apple harvesting requires precise integration of visual sensing and mechanical manipulation subsystems. Figure 3 displays the logical sequence of various processes within the integrated system. At the beginning of each harvesting cycle, the RGB-D (Red, Green, Blue, and Depth) camera system detects and localizes every apple within the system's field of view. After prioritization, fruit coordinates are passed to the mechanical system, thus visual sensing and manipulation are combined in an open-loop fashion where the system first "looks" then "moves." Because all fruit in the scene are identified at the beginning of a cycle with no additional visual sensing between successive fruit picks, the vision system is described and will be referred to as a global camera setup henceforth. A seven DOF manipulator with an under-actuated, passively compliant end-effector approaches, grasps, and detaches fruit from the tree. Fruit grasping is executed with open-loop control. Picking is continued until all prioritized apples are removed from the scene marking the end of a harvest cycle. More detailed explanations of subtask execution are provided in the following sections.

6 | MACHINE VISION SYSTEM

6.1 | Global camera system and apple identification

For this research, the machine vision algorithm developed by Silwal et al.^{29,30} was used for fruit identification. In brief, this algorithm uses

Circular Hough Transformation (CHT) to identify clearly visible as well as individual apples in clusters and Blob Analysis (BA) in an iterative fashion to identify partially visible apples. It has been previously tested in clustered and complex canopy structures with a fruit identification accuracy greater than 90%.

A common machine vision setup in a robotic fruit harvesting system consists of a camera attached to the manipulator or end-effector.^{49,52} The single global camera system used in this research requires imaging only once at the beginning of the cycle to identify and localize the apples. This approach saves time compared to repetitive imaging required in visual servoing and increases the overall efficiency of the system. The machine vision system consisted of a single CCD (Charged Couple Device) color camera (Prosilica GC1290C, AVT Technologies, f/1.4-6 mm lens with 43.6° horizontal and 33.4° vertical field of view) mounted on top of a time-of-flight based 3D camera (Camcube 3.0, PMD Technologies, f/1.1-12.8 mm lens with 40° x 40° fields of view). The goal of this configuration was to acquire color images with the CCD camera to identify the apples and then obtain their 3D coordinates from the point cloud acquired by the 3D camera. Currently, the vision system uses a black curtain as a uniform background to facilitate image segmentation as described in Section 9.

6.2 | Exposure fusion

Variable lighting is one of the most perturbing factors for vision systems operating in outdoor environments such as orchards. Natural daylight conditions result in images having irregular exposures that alter color saturation and contrast. In extreme cases, highly over/under-exposed images can negatively impact fruit identification. To overcome this limitation during field trials, an exposure fusion technique developed by Mertens et al.⁵³ was used. This technique computes a well-exposed image by keeping only the best regions of each image from a multiple exposure image sequence. Image quality parameters such as contrast, saturation, and well-exposedness are used to compute the best regions and weight the blended image stack into a final image. Implementation of this process created a uniformly exposed image of apple tree canopies while minimizing shadows. Figure 4 shows the multiple exposure sequences and its fusion result.

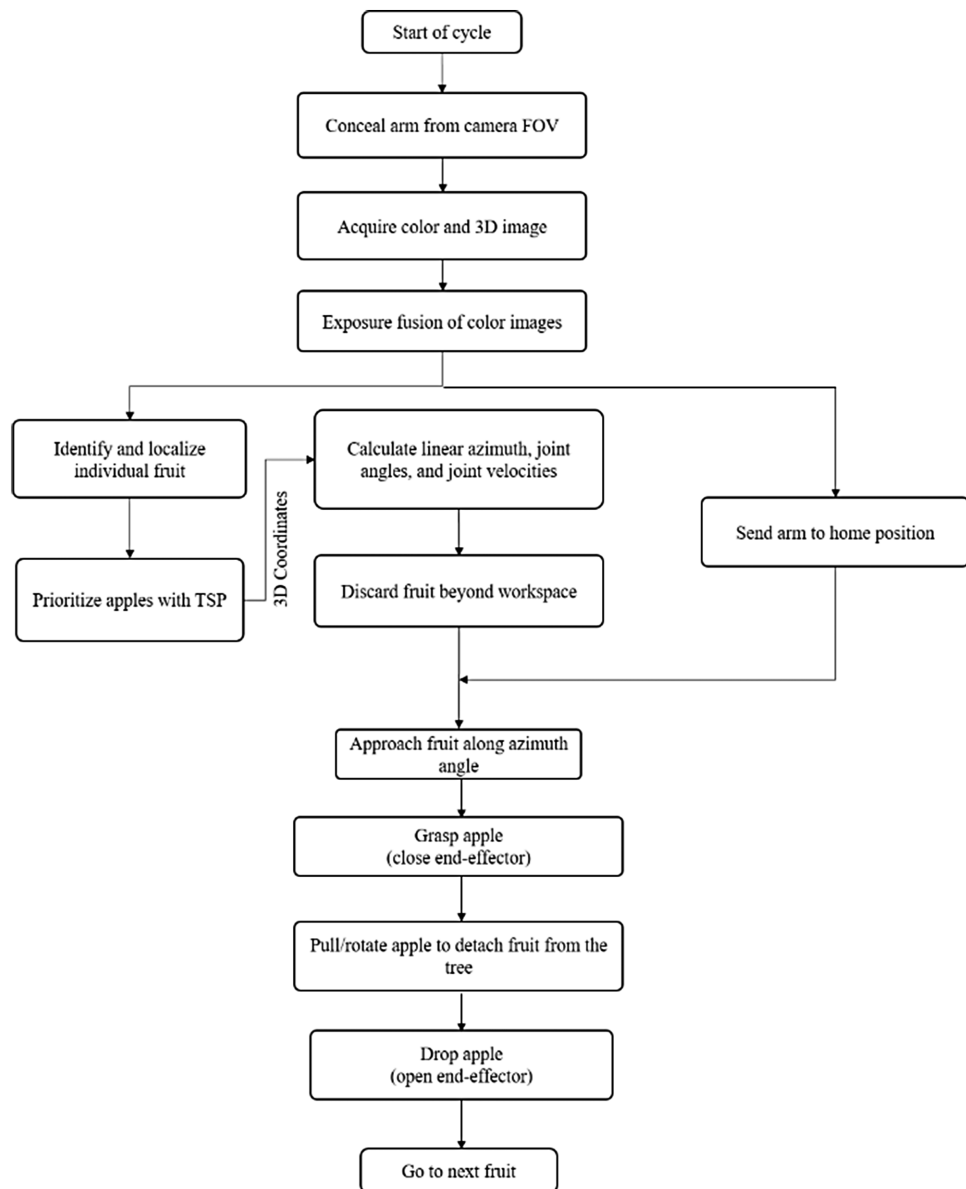


FIGURE 3 Task logic for a single harvesting cycle. When possible, parallel threads were used to execute operations in parallel in order to minimize overall harvesting time

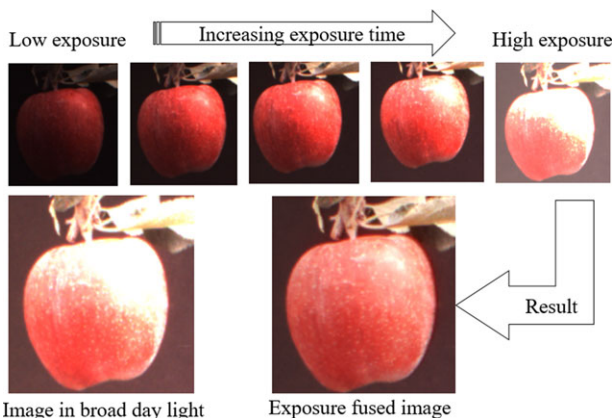


FIGURE 4 Exposure sequence showing a set of five images at increasing exposure level (upper row). The exposure fused image is compared to a regular image obtained in broad daylight (lower row)

In total, five images with different exposure values were taken for exposure fusion. To incorporate a wide range of exposure values, the image exposure time was sequenced in increasing order starting from an under-exposed time (4 ms) to a highly exposed time (45 ms). The total time required to capture all five images was approximately 0.34 s with an average time of 68 ms per image. The under-exposed images contributed toward reducing saturated regions whereas the highly exposed samples reduced the effect of shadows and poorly lit areas in the images.

6.3 | Camera calibration and hand-eye coordination

In the vision system, the color camera was positioned above the 3D camera. This configuration is similar to a stereo vision system that requires intrinsic and extrinsic parameters to map 3D information into a 2D color image. Intrinsic parameters including focal length, principle

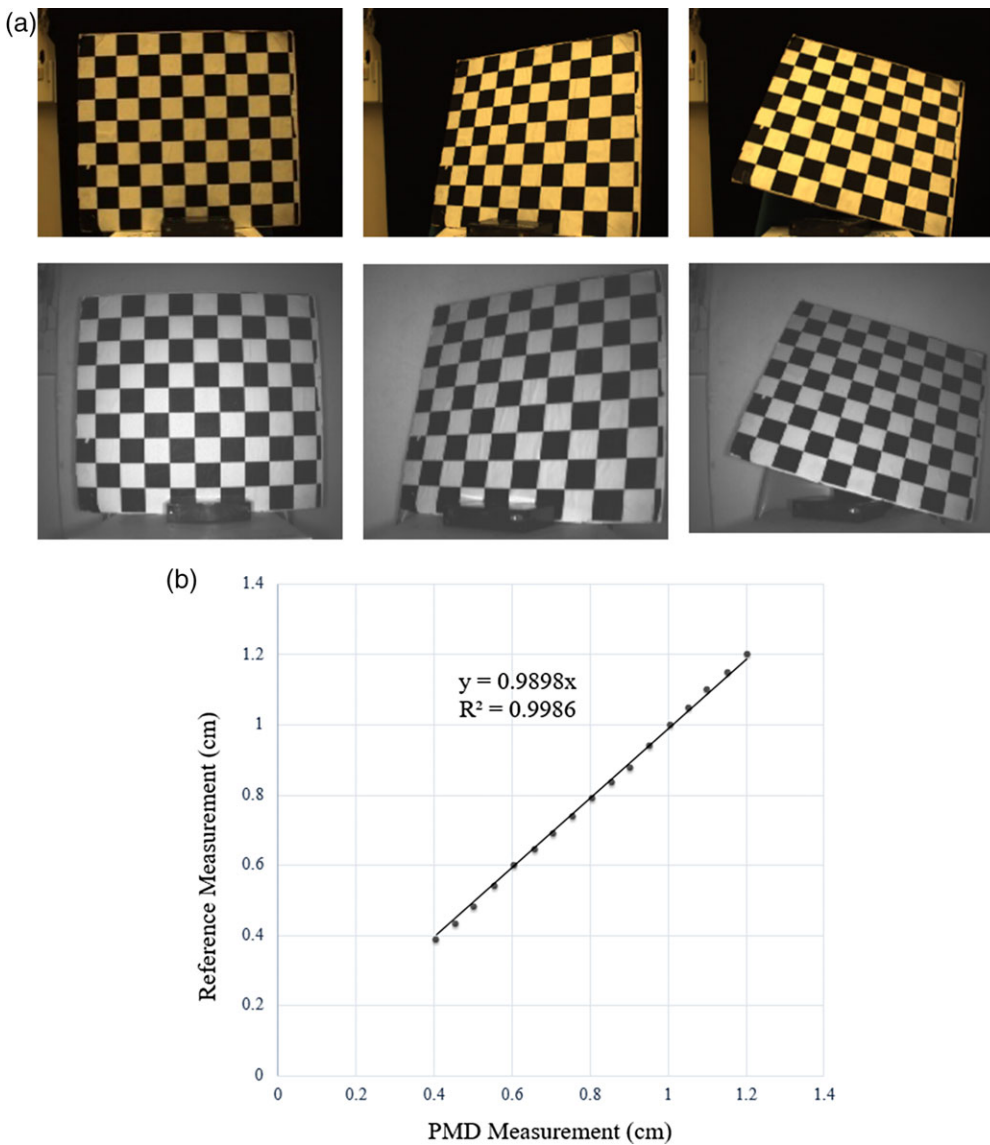


FIGURE 5 Camera calibration using checkerboard pattern and handheld laser

point, and distortion coefficient (skew, radial and tangential) as well as extrinsic parameters such as camera translation and rotation matrices were obtained using Matlab's (Mathworks, Natick, MA) camera calibration toolbox⁵⁴ and a checkerboard (9×7 squares, each square measuring $0.05\text{ m} \times 0.05\text{ m}$). A few instances of the checkerboard calibration process are shown in Figure 5(a). Intrinsic parameters were used to remove distortion from both cameras whereas extrinsic parameters were used to inverse map the 3D point cloud onto the color image using the equation shown below

$$\begin{aligned} U_{RGB} &= f_{x, RGB} * X' / Z' + C_{x, RGB} \\ V_{RGB} &= f_{y, RGB} * Y' / Z' + C_{y, RGB} \end{aligned} \quad (1)$$

where U_{RGB} and V_{RGB} are coordinates of the 3D pixels mapped into the RGB image, X' , Y' and Z' are 3D coordinates with respect to the RGB camera, $f_{x, RGB}$ and $f_{y, RGB}$ are focal lengths in the x and y-axis for the color camera, and $C_{x, RGB}$ and $C_{y, RGB}$ are the camera centers along the x and y-axis, respectively. A similar work by Van den Bergh and

Van Gool,⁵⁵ involved fusion of a low-resolution 3D image with a high-resolution 2D color image for 3D hand gesture interaction.

After stereo and individual camera calibrations, an additional calibration step was required to verify depth measurements from the 3D camera. A handheld laser range finder with a precision of 0.1 mm was mounted along the PMD camera's principle axis to measure the precise distance from the PMD sensor position to a 3D object. The distance to the same spot on the object was then measured using the PMD camera to compare and estimate the accuracy of the 3D camera. This comparison was repeated for various distances between 0.5 m and 1.5 m, which were representative distances from the camera to the fruit during field experiments. A regression plot showing a highly linear relationship with the absolute reading is provided in Figure 5(b). Additionally, as described by Ringbeck and Hagebeuker,⁵⁶ and Möller et al.⁵⁷ ToF camera accuracy in bright lighting conditions also depends upon the proper selection of integration time (demodulation amplitude) to minimize pixel failure. 3D camera measurements were compared with handheld laser depth measurements at different values of integration

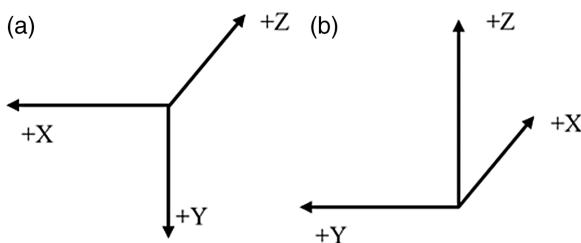


FIGURE 6 Difference in axis orientation between PMD with the left-hand coordinate system (a) and manipulator (b) with the right-hand coordinate system

time to select the most appropriate integration time. From this experimental integration time of 200 microseconds was found to be most appropriate. On average, at a distance of 1.5 meters, which was the maximum allowed distance from the apples to the camera during field testing, the measurement's standard deviation was 6 mm.

In the experimental setup the robotic arm was directly in front of the camera system. In this setup, the longitudinal axis of the camera and manipulator were aligned to the same axis. The coordinate systems of the camera and manipulator are shown in Figure 6. With this arrangement, a simple translation was used to transform 3D camera coordinates to the manipulator's reference frame. The transformation matrix was

$$\begin{bmatrix} X_{\text{manipulator}} \\ Y_{\text{manipulator}} \\ Z_{\text{manipulator}} \end{bmatrix} = \begin{bmatrix} a \\ b \\ c \end{bmatrix} + \begin{bmatrix} Z_{\text{pmd}} \\ X_{\text{pmd}} \\ Y_{\text{pmd}} \end{bmatrix} \quad (2)$$

where a, b and c are constants obtained from calibration. Apples were placed at four known locations to the manipulator and centered to the end-effector's palm. Then, the 3D camera was used to obtain the location of the center of each apple. Equation (2) was then used to inversely calculate the transformation matrix coefficients (i.e., a, b, and c) for each point. The coefficient averages from the four apples were used for all other transformations. The end-effector was designed to have robustness to position error for compensating 3D measurement deviation as described in Section 7.

6.4 | Fruit localization

Figure 7 shows an example output of the machine vision system used in this work. Figure 7(a) shows the fusion of color and the 3D point cloud with depth filtering. 3D point clouds marked as blue dots are layered on top of the color images. Two of the apples in Figure 7(a) have no overlaid 3D locations because they were significantly farther from the camera. A similar logic is visible in Figure 7(b) where the fruit identification algorithm has circled all apples in the image except those too far away. 3D coordinates mapped and present inside these green circles were then averaged to calculate the mean x, y and z coordinates of the respective apples. A statistical outlier removal technique (modified Thompson rule) was used to remove coordinates with significant deviation in depth values. Figure 7(b) also displays the results of fruit prioritization (see Section 8.1) by assigning the harvesting priority on each apple.

During the field experiment, a plain black background was manually inserted behind the tree canopy before field studies. The purpose of the black curtain was to facilitate image segmentation as it is often considered as primary source of error in vision (see Section 2) and affects subsequent processes.⁴⁸ The background in the apple canopy when the curtain was not used contained the sky, the canopy from adjacent rows, and the ground surface as additional objects to be segmented before identifying fruit. Use of the curtain had the potential to simplify image segmentation and improve vision robustness by providing a uniform background. The opaque curtain had minimal effect on variation of lighting penetrating the canopy except in the morning when it blocked light directly forward of the camera. The experiments were conducted at various times of the day. In our earlier research,²⁹ we proposed an over-the-row platform that had opaque curtains providing a controlled lighting environment and black background. The black curtain used in this study is representative of the uniform background present inside the over-the-row platform. Future studies with the robotic harvester will be conducted using this supportive structure. Such a structure could also provide both day and night time capabilities for robotic harvesting.³⁰ This previous work showed no statistical difference in vision performance between day and night using the over-the-row platform.

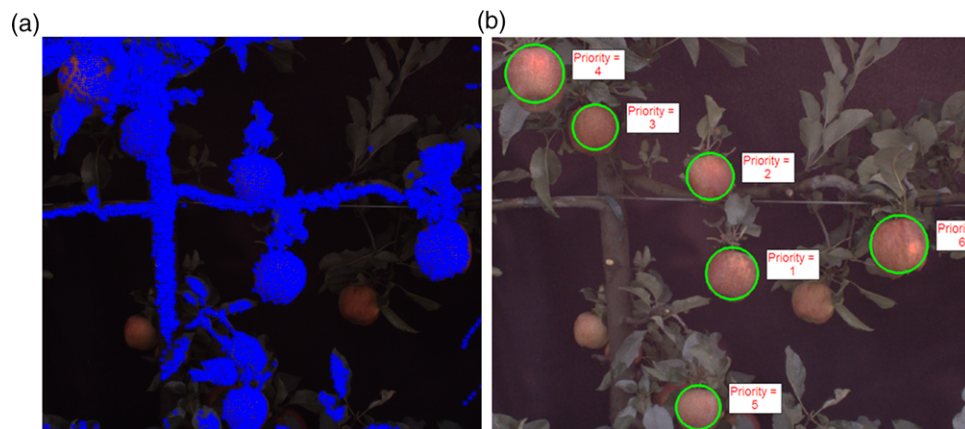


FIGURE 7 Vision system results showing 3D coordinate mapping (a), apple identification and picking prioritization with TSP (b)

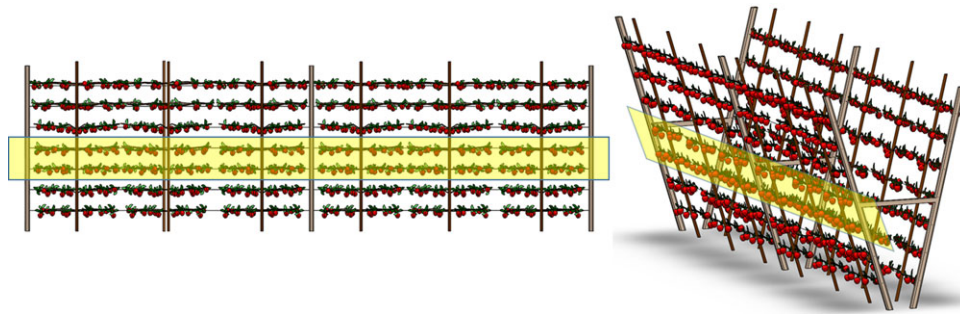


FIGURE 8 Two different views of the system's working environment (shaded regions) in relation to tree structures

7 | MECHANICAL DESIGN

Based on orchard parameters and 0.94 m bed height of the mobile platform (Section 9) used for field studies, the third and fourth trellis wires were selected as the working environment for the mechanical design. The intent was to assess the overall approach and determine what additional functionality was needed, if any, before expanding the system to the entire tree. The shaded regions in Figure 8 show the working environment in relation to tree geometry. The robotic harvester's mechanical design includes a custom, serial link manipulator with seven DOF and a grasping end-effector.

7.1 | Manipulator

It is important to note that manipulator optimization for agricultural harvesting applications is an active area of research.^{58–61} Kinematic optimization early in the design process to produce a universal design is challenging because of significant variations between tree systems and fruit distributions, even in the same orchard. A secondary objective of this research is to identify environmental parameters, like, for example, trellis wire spacing, fruit density, fruit distribution, and pruning practices, that would produce an optimal environment for robotic harvesting. Collaboration with growers and horticulturalists to produce these optimized biological systems, which may reduce the DOF required in a commercial model, is ongoing.

To expand the number of permissible end-effector orientations at the target fruit's position and not constrain the approach path (e.g., horizontal only), a manipulator task space $\mathcal{T} \subset SE(3)$ was desired. Monte Carlo simulations were conducted to determine links lengths for a six DOF conceptual model. Matlab's (Mathworks Inc., Natick, MA) random number function was used to generate a 100000×1 vector of uniformly distributed random numbers for each joint within its respective joint limits. For each row of joint coordinates, the manipulator's forward kinematics was then used to determine the position of the end-effector. Simulation results were used to graphically verify that the resulting workspace bounded the region between the third and fourth trellis wires (Fig. 8) in the vertical direction.

Further lab studies with the fabricated six DOF arm and a replica apple tree⁶² indicated the need for a seventh degree of freedom. Unlike a vertical orchard system, in the V-trellis system selected for field studies apples on the far side of the canopy plane are not

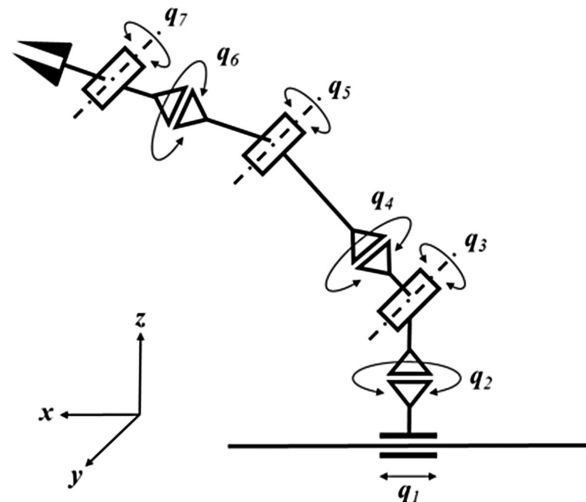


FIGURE 9 Kinematic model of the prototype manipulator developed for the robotic apple harvester

accessible from the adjacent row. A prismatic base was added to extend the depth of the reachable workspace into the tree canopy. As will be shown in Section 8, the kinematic redundancy provided by the seventh degree of freedom was used to help the manipulator avoid singularities during fruit picking. The kinematic model of the serial link manipulator is provided in Figure 9.

The CAD model of the system's complete mechanical design is shown in Figure 10. Because the system is an active research platform, a modular design providing flexibility for configuration changes was also required. Dynamixel Pro actuators (Robotis Inc., Irvine, CA) were selected for the all-revolute arm because their modularity simplified component integration. The manipulator uses two each H54-200, H54-100, and H42-20 Dynamixel Pro models. The manipulator's two link frames were fabricated from 11 gauge aluminum sheet metal using a water jet cutter and sheet metal bender. The lengths of links one and two are 0.20 m and 0.14 m, respectively. The six DOF manipulator is fastened to a prismatic base, which consists of an aluminum plate secured to four bearing blocks mounted on 16 mm diameter linear rails. The rails are 55 cm long case hardened shafts. The prismatic base's actuator is a bipolar NEMA 23 stepper motor coupled to a series of pulleys with a timing belt. Some of the mechanical system's basic performance parameters are reported in Table 2.

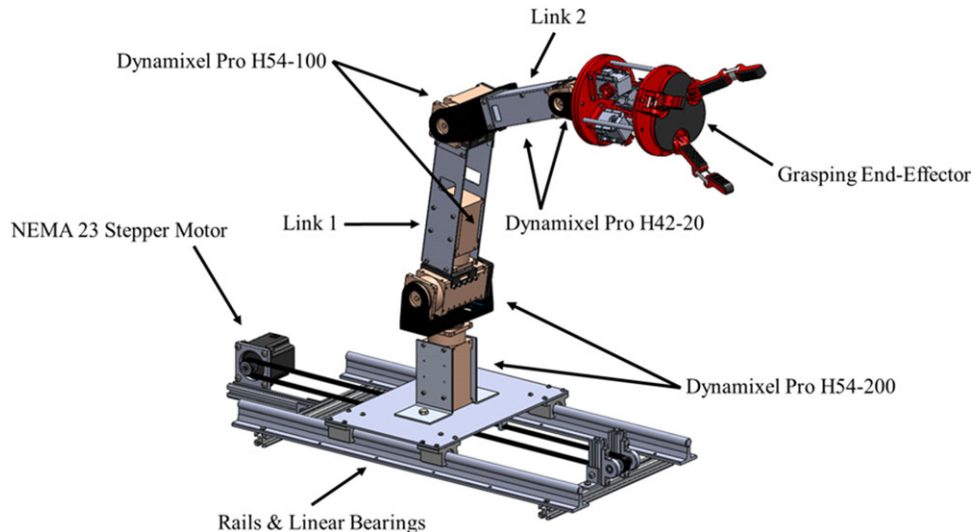


FIGURE 10 CAD model of the 7 DOF robotic system with grasping end-effector. The 6 DOF, serial link manipulator is mounted on a prismatic base

TABLE 2 Key specifications for the seven DOF mechanical design

Parameter	Value
Link 1 Length	0.20 m
Link 2 Length	0.14 m
Outstretched Arm Length ^a (including end-effector)	0.67 m
Max Velocity: Joint 1	0.10 m/s
Max Velocity: Joints 2–7	120 deg/s
Approximate Payload	2.5 kg
Manipulator Voltage	24 V
Rated Power	700 W

^aWhen the arm is parallel to the axis of the prismatic base

7.2 | End-effector

The harvesting end-effector is the only system component that makes physical contact with the fruit. The fruit removal technique selected during this research incorporates a grasping end-effector. An advantage of a grasping approach is control over the end-effector workspace dimensions. Unlike a vacuum and funnel design with a constrained opening span, for example, there is the potential for incorporating grasp planning for apples in especially cluttered environments, such as clustered fruit or those adjacent to obstacles. Development of the end-effector and fruit picking motion was facilitated by a recent study of the hand picking process.²⁰ During this study, a human operator applied a three-fingered grasp to assess the efficiency of four apple-picking patterns not selective to stem orientation. The picking patterns considered were horizontal pull, horizontal pull and twist, inclined pull, and inclined pull and twist. Force sensors on the fingers and an inertial measurement unit (IMU) installed on the hand were used to measure peak distal normal forces at the point of fruit separation from the tree, angle of fruit rotation at separation, and total displacement from the onset of motion to separation.

The end-effector design (Fig. 11) is an underactuated, tendon-driven device designed to produce a spherical power grasp⁶³

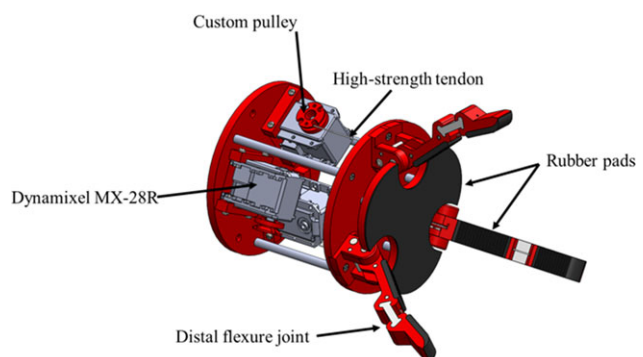


FIGURE 11 CAD model of the apple-picking end-effector. The design includes three identical tendon-driven fingers with two links each and a total of three actuators

providing form-closure of the fruit. Underactuation is incorporated to provide a grasp adaptive to apples with asymmetrical geometries and variable orientations. Three identical fingers with two links are arranged symmetrically around a palm. The fingers are modified versions of the open source design⁶⁴ used on the iRobot-Harvard-Yale hand.⁶⁵ For actuation, each finger tendon is attached to a Dynamixel MX-28R actuator (Robotis Inc., Irvine, CA). Soft polyurethane pads on the palm and finger links help minimize fruit bruising and increase friction forces during grasping.

Another mechanical feature incorporated in the end-effector design is passive compliance. The distal joint is a passively compliant flexure. Dollar and Howe⁶⁶ have shown that passive compliance significantly increases grasp robustness to error acquired during perception of the target object's position. An additional advantage of the flexure for harvesting applications is that its out-of-plane compliance helps minimize damage during unintended collisions.⁶⁶ The proximal joint is a single DOF pin joint. A torsion spring in the proximal joint provides the return action when tendon tension is relaxed. All structural components on the end-effector were fabricated from solid models by a Replicator 2X printer (MakerBot Industries, New York). The distal

flexures were printed with flexible filament (Fenner Drives, Lancaster, PA). Additive manufacturing helped reduce the weight of the device as well as minimize the number of fasteners required for assembly. Excluding the mass of the mounting plate used to fasten the end-effector to the manipulator, the total mass of the device is 0.63 kg. Considering the mean mass of the apple (Table 1), the total expected payload is less than 1 kg. Additional information about the analysis, design, and fabrication process used to build an earlier end-effector prototype can be found in the recent paper by Davidson and Mo.⁶⁷

The end-effector does not contain any sensors and grasping is executed in a purely open-loop manner with feedforward control. Each finger actuator is preset to a torque value with a limiting stall current. Finger motion stops when the actuator's encoder indicates that the motor has stalled. Because the actuator is non-back drivable, reducing the motor current to a small amount is sufficient to ensure that tendon tension is maintained. After a grasp is initiated, the system waits for a small amount of time assuming that static equilibrium is reached with the grasped fruit. To release the apple the direction of motor rotation is reversed and the finger is returned to a preset open position. This control mode was selected to reduce design costs and complexity as well as increase manipulation speed.

8 | HARVESTING CYCLE ACTIVITIES

After fruit localization, all apples identified in the scene are prioritized so as to optimize the picking sequence. The system then determines manipulator joint solutions for a set of waypoints along the path to each fruit. The end-effector's path to and from each apple is linear. A limitation of the design used during field studies is that the potential provided by kinematic redundancy was not fully exploited. In order to reduce cost, a low-cost stepper motor ($\sim \$30$ USD) was selected for the prismatic base's actuator. Overall manipulation speed was constrained by the stepping frequency required to provide torque sufficient to displace the arm. Therefore, as will be described in Section 8.2, during field studies the inverse kinematics (IK) planner prioritized motion of the six DOF arm. The stepper motor was replaced with a high torque Dynamixel Pro actuator after the harvesting window was complete. Modifying the inverse kinematics planner to solve the redesigned system's inverse kinematics on the velocity level using well-established algorithms for redundant manipulators is ongoing.⁶⁸

8.1 | Apple prioritization

This research considers the task of apple prioritization during each harvesting cycle as a traveling salesman problem (TSP). The TSP is a well-known optimization problem in the class of Non-Deterministic Polynomial-Time hard (NP-hard) problems. In brief, the TSP aims to find a route from a known location that visits a pre-described set of locations, visiting each only once, and returns to the original location in such a way that the total traveling distance is minimum. The Nearest Neighbor algorithm⁶⁹ was used to solve the TSP where distances between apples were calculated using the 3D Euclidean distance

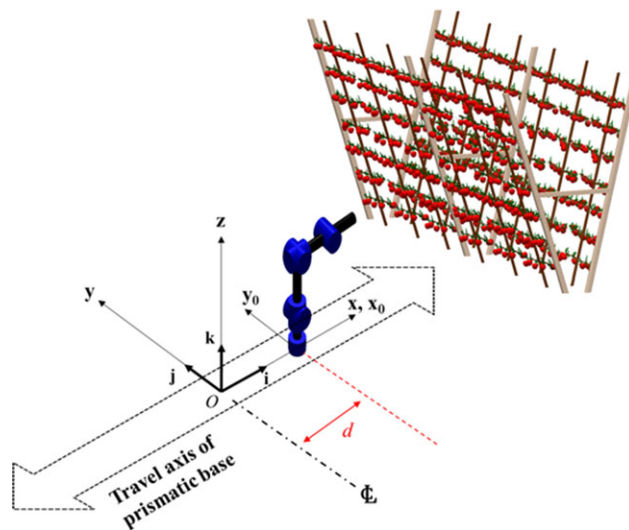


FIGURE 12 The world reference frame of the autonomous harvesting system is located at the prismatic base's centerline

equation with respect to the manipulator's starting location at the beginning of a harvesting cycle.

8.2 | Path planning

This section describes path planning for a single fruit pick. The origin of the world reference frame O (a right-hand coordinate frame) with unit vectors i, j, k is located at the arm's base where it is centered over the mobile platform (Fig. 12). The world x -axis is oriented along the length of the mobile platform normal to the tree canopy and the world z -axis is vertical. Using pure translation, the fruit's position vector is transformed from the camera's reference frame to the world reference frame O . Let $\mathbf{p} = (a+d)\mathbf{i} + b\mathbf{j} + c\mathbf{k}$ be the vector of coordinates of the fruit's center with respect to frame O where d is displacement of the prismatic base along the x -axis. At the beginning of IK planning the arm's base frame B with unit vectors x_0, y_0, z_0 ⁷⁰ is collocated and aligned with the world reference frame O (i.e., d is equal to 0). The motion planning algorithm determines the six DOF arm's inverse kinematics (IK) using the dual optimization technique proposed by Wang and Chen.⁷¹ In brief, the cyclic coordinate descent (CCD) method⁷² is used to rapidly find a joint vector \mathbf{q} near the true solution, which is then used as input to the Broyden–Fletcher–Goldfarb–Shanno (BFGS) variable metric method⁷² to obtain a solution at the desired degree of precision. The joint limits of the manipulator are used as boundary constraints and the convergence tolerance of the objective function is set at 1E-6. For each apple in the harvesting cycle, inverse kinematics solutions are found for three positions, the approach point, grasp point, and release point. The prismatic base is only displaced if the IK solver fails to converge to a solution for the desired end-effector position, or if the manipulator's configuration at the apple's position is near a singularity. The algorithm then performs a search along the axis of the prismatic base to find a displacement d that leads to an IK solution, if any. The end-effector's path and velocity between the three positions are specified in the operational space.

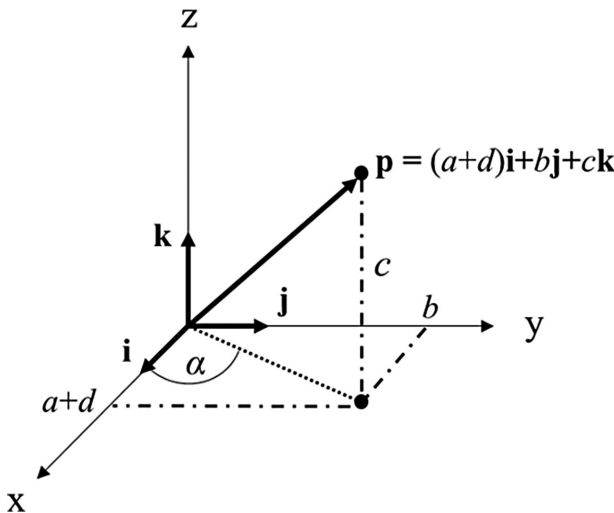


FIGURE 13 The azimuth angle partially defines the orientation of the end-effector's normal vector at the approach position

8.2.1 | Approach to fruit

The approach point is 15 cm from the fruit. At the approach position the orientation of the end-effector's normal vector \mathbf{n} is partially defined by an azimuth angle α , which is the angle between the x -axis and the projection of \mathbf{p} in the x - y plane (Fig. 13). So, the equation for the azimuth angle α is

$$\alpha = \tan^{-1} \left(\frac{b}{a+d} \right) \quad (3)$$

The path the end-effector follows to the apple depends on fruit height. If c is less than 0.55 meters, the end-effector makes a horizontal approach to the fruit. To expand the number of apples that can be picked, the end-effector follows a 45° inclined path to fruit that are vertically higher than 0.55 meters. For the horizontal approach, the rotation matrix \mathbf{U}^E relating orientation of the end-effector's frame E with respect to the manipulator's base frame B is obtained via the elementary rotation matrix about the z -axis $\mathbf{R}_z(\alpha)$. For the inclined case, \mathbf{U}^E is found by composition of elementary rotations about the y and z coordinate axes

$$\mathbf{U}^E = \mathbf{R}_z(\alpha) \mathbf{R}_y(-45^\circ) \quad (4)$$

8.2.2 | Fruit grasp

Before selecting the joint vector \mathbf{q} required for the end-effector to reach the apple, the motion planning algorithm first checks the kinematic configuration of the arm at the fruit's position. The geometric Jacobian $\mathbf{J}(\mathbf{q})$ of the differential kinematics equation defines a linear mapping⁷³

$$\mathbf{v}_e = \mathbf{J}(\mathbf{q}) \dot{\mathbf{q}} \quad (5)$$

between the arm's 6×1 vector $\dot{\mathbf{q}}$ of joint velocities and the 6×1 vector $\mathbf{v}_e = [\mathbf{l}_e \omega_e]^T$ of linear \mathbf{l}_e and angular end-effector velocities ω_e in the arm's base frame B . Because end-effector velocity from the approach point to the grasping point is defined relative to the end-effector frame

E , the algorithm first computes the geometric Jacobian $\mathbf{J}^E(\mathbf{q})$ in frame E using the relative rotation matrix \mathbf{U}^E whereby

$$\mathbf{J}^E(\mathbf{q}) = \begin{bmatrix} \mathbf{U}^E & \mathbf{0} \\ \mathbf{0} & \mathbf{U}^E \end{bmatrix} \mathbf{J}(\mathbf{q}) \quad (6)$$

The motion planning algorithm then checks the condition number of the 6×6 matrix \mathbf{J}^E . For an ill-conditioned Jacobian \mathbf{J}^E , the algorithm updates the prismatic base position in an iterative fashion until the arm's configuration is optimized to produce higher end-effector velocities at the apple's position.

The end-effector's velocity from the approach to apple position is $0.15 \text{ m}\cdot\text{s}^{-1}$ along its normal vector \mathbf{n} , the orientation of which was defined by the azimuth angle α . So, for the horizontal and inclined approach $\mathbf{v}_e^E = [0.15 \ 0 \ 0 \ 0 \ 0 \ 0]^T (\text{m}\cdot\text{s}^{-1})$ where \mathbf{v}_e^E is the end-effector velocity expressed in the end-effector frame E . The required joint velocities $\dot{\mathbf{q}}$ are found with the inverse differential kinematics equation using the vector of joint angles of the manipulator's configuration when the end-effector is at the approach position

$$\dot{\mathbf{q}} = (\mathbf{J}^E(\mathbf{q}))^{-1} \mathbf{v}_e^E \quad (7)$$

The algorithm used for computation of the system's kinematics at the grasping position is shown below. The initial base position d is the displacement of the prismatic base at the approach position. End-effector orientation and velocity are determined by the azimuth angle and fruit height. If a solution of real joint variables and a well-conditioned geometric Jacobian are not found, the base position is incremented alternating between positive and negative displacements. Between each iteration the algorithm checks for acceptable results. Should a solution of real joint variables and well-conditioned Jacobian not be found within the range of the mobile base, which is approximately 0.44 m, the fruit is excluded from the picking cycle.

Algorithm 1.

Input: Fruit position \mathbf{p} ; relative rotation matrix \mathbf{U}^E for desired end-effector orientation; desired end-effector velocity \mathbf{v}_e^E ; initial base position d

Output: 6×1 vector of joint angles \mathbf{q} ; 6×1 vector of joint velocities $\dot{\mathbf{q}}$; final base position d ;

temp = 1;

for $i = 1:12$

- Call IK solver(\mathbf{p}, \mathbf{U}^E) $\rightarrow \mathbf{q}$
- Call FK solver($\mathbf{q}, \mathbf{v}_e^E$) $\rightarrow \mathbf{J}^E$ and $\dot{\mathbf{q}}$
- if** $\mathbf{q} \in \mathbb{R}$ **&&** cond(\mathbf{J}^E) $<= 40$

 - break;

- end**
- $d = \text{temp} * (0.01 * i)$;
- $\text{temp} = -\text{temp}$;

end

8.2.3 | Release of fruit

After grasping the apple, the manipulator moves the end-effector 12 cm back from the tree along a path coincident with the

end-effector's normal vector \mathbf{n} originally defined by the azimuth angle and fruit height. Selection of the 12 cm displacement was based on previous studies of fruit picking dynamics,²⁰ which showed that mean displacement to fruit separation from the onset of picking was approximately seven cm. The end-effector's linear velocity \mathbf{L}_e^E along the path to the release point has the same magnitude as the linear velocity from the approach position to the grasping position. During fruit detachment, there is also a 45° rotation (0.6 rad·s⁻¹) around \mathbf{n} in order to produce a combined pulling and twisting motion. The rotation matrix \mathbf{U}_R^E relating orientation of the end-effector's frame E to the manipulator's base frame B at the release point is therefore

$$\mathbf{U}_R^E = \mathbf{R}_z(\alpha) \mathbf{R}_x^E(-45^\circ) \quad (8)$$

for the horizontal approach/removal and

$$\mathbf{U}_R^E = \mathbf{R}_z(\alpha) \mathbf{R}_y(-45^\circ) \mathbf{R}_x^E(-45^\circ) \quad (9)$$

for the inclined approach/removal where \mathbf{R}_x^E is the elementary rotation matrix about the x -axis of frame E (i.e., the end-effector's normal vector \mathbf{n}). The position and orientation at the release point are passed to the IK solver for calculation of the required manipulator joint angles \mathbf{q} .

9 | EXPERIMENTAL SETUP FOR FIELD EVALUATION

Figure 14(a) shows the setup used during field testing of the robotic system. Supporting equipment such as cameras, laptop, manipulator, and other electrical components were mounted on the cargo box of a John Deere Gator electric utility vehicle (John Deere, Moline, IL, USA). Of note, the robotic system was assembled on sliding aluminum profile to simplify setup requirements during field trials. The imaging system was placed directly behind and above the manipulator, on average, a meter and a half away from the trellis wires in the tree canopies. The home location of the robotic arm was half a meter closer to the canopy. All electrical components were powered by a 5000 W mobile generator. The required stepdown (110 VAC to 12/24 VDC) power supplies were used to drive the DC stepper motor and servo motors. The mobile testing platform was driven between orchard rows to acquire static color images and execute a harvesting cycle. As the robotic arm was directly in front of the camera system (Fig. 14a) at the beginning of a harvesting cycle, the manipulator was concealed from the camera's Field of View (FOV) during imaging. In order to assess robotic picking functionality, the vehicle remained stationary while imaging and picking apples and was then driven by a human operator to the next harvesting point in this field test. Weather conditions during field studies were partly cloudy to sunny, minimal wind, and temperatures ranging from 10 to 20° C. Field studies were conducted during both night and day lighting conditions.

The hardware architecture (Fig. 14b) of this robotic platform primarily consisted of a global camera system, a 7-DOF manipulator, and a grasping end-effector connected and centrally controlled by a laptop. Figure 14(b) also shows the complete hardware architecture and

communication linkage between different peripherals used in this project. The nine Dynamixel actuators (six on the arm and three on the end-effector) were interfaced to the laptop via a USB adapter (Robotis Inc., Irvine, CA) with RS-485 communication protocol. These high precision motors were programmatically controlled using the Software Development Kit (SDK) provided by Robotis Inc. The bipolar stepper motor and its micro-stepping driver (SainSmart, Lenexa, KS, USA) on the mobile base were connected to the computer via an interface board from Phidgets Inc. (Calgary, Canada). Additionally, the PMD camera and color camera were connected via USB and ethernet cables. Use of the respective SDKs and communication protocols for each hardware interface is shown in Figure 15.

As seen in Figure 15, programming flow frequently switches between Matlab and the C++ domain. The vision algorithm²⁹ and path planning algorithm were primarily developed in Matlab utilizing its programming efficiency and inbuilt supports for prototype development. On the other hand, a stable communication base with each hardware component was separately developed in C++ using support packages from individual manufacturers. This hybrid programming approach incorporates the advantages of both the Matlab and C++ environments, namely, efficiency and stability, respectively. The Matlab Engine was used as a bridge to transfer information between these programming domains. In general, acquired color images and 3D point clouds were transferred to Matlab for fruit identification, 3D localization, prioritization, and inverse kinematics calculations. Then, the joint angles and velocities for each identified apple were transferred back to the C++ environment for generation of the appropriate control signals needed to manipulate the robotic arm and base. A PC configured with an Intel Core 2 Quad processor at 2.66 GHz clock rate, 4 GB RAM, and Windows 7 64-bit Operation System was used for processing the machine vision algorithm as well as all other subroutines. A substantial improvement in computational speed may be possible with optimization of code and use of a singular programming platform, as well as hardware (Graphics Processing Unit) and software architectures.

10 | RESULTS

10.1 | Machine vision system

A total of 54 harvesting cycles were completed. As vision was required only once at the beginning of each cycle, the total number of images acquired was equal to the total number of harvesting cycles. After selective thinning of apples as described in Section 4, the manual count of apples in the 54 images totaled 193 fruit with an average distribution of four apples per image. In total, the vision system was able to accurately identify all 193 apples resulting in a fruit identification accuracy of 100% under variable lighting at different times of the day.

10.2 | Manipulation

Of the 193 apples identified, 150 of the fruit were in the system's reachable workspace and were selected as the harvesting samples in this study. The picking efficiency for the apples the system attempted to pick was 84.6% (127/150). Figure 16 shows the end-effector

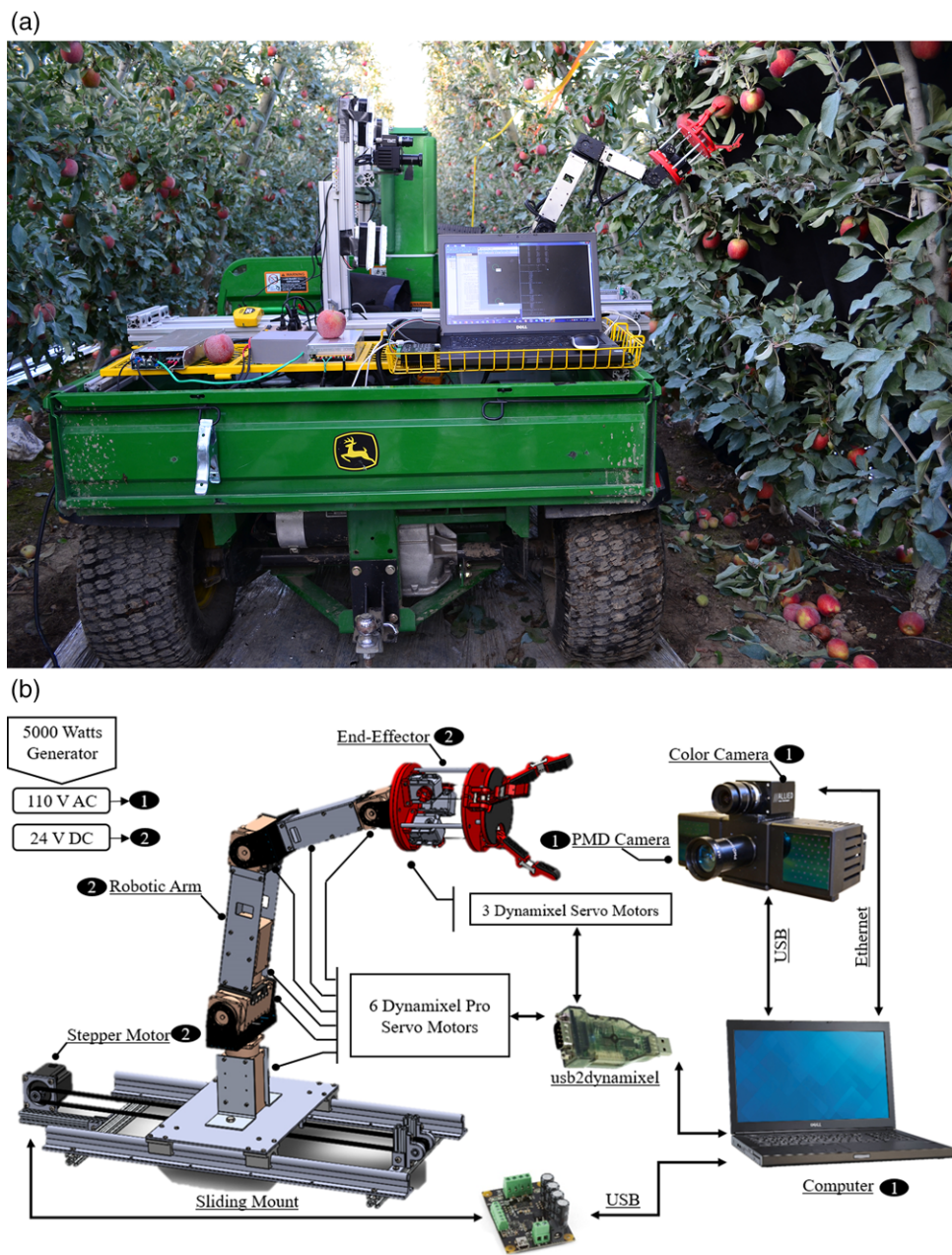


FIGURE 14 The robotic platform with the arm attached to end-effector, global camera system and computer during field testing (a). Hardware architecture indicating voltage system, individual part location and communication protocol (b)

successfully grasping a sample fruit. The causes of the 23 missed fruit were analyzed and grouped into five categories:

1. Position and/or calibration error (34.8%)—The most frequent cause of missed fruit was a missed grasp due to the accumulation of position error during fruit localization.
2. Poorly thinned branch (30.5%)—This category describes fruit that grew on long, thin shoots and were located up to 0.4 m below the trellis wire. In this situation, the fruit would swing like a quasi-pendulum away from the canopy during the end-effector's removal path. Then, the fruit would either not detach from the tree or would remain in the end-effector and interfere with the next fruit pick in the cycle. Figure 17 shows an example fruit from this category.

3. Obstruction (13.0%)—On three occasions the end-effector was not able to complete its grasp of the fruit because one of the device's fingers obstructed an interfering obstacle like a branch or sprinkler line.
4. Previous fruit stuck in end-effector (13.0%)—On several occasions, the spur detached with the fruit and was caught in the device, so the previous apple remained in the end-effector when it went to grasp the next fruit in the cycle.
5. Incomplete detachment (8.7%)—The system could not detach two of the fruit that it successfully grasped (i.e., the fruit slipped from the grasp). Based on visual observation of fruit color, the apples appeared to be immature; they were difficult to pick by hand.

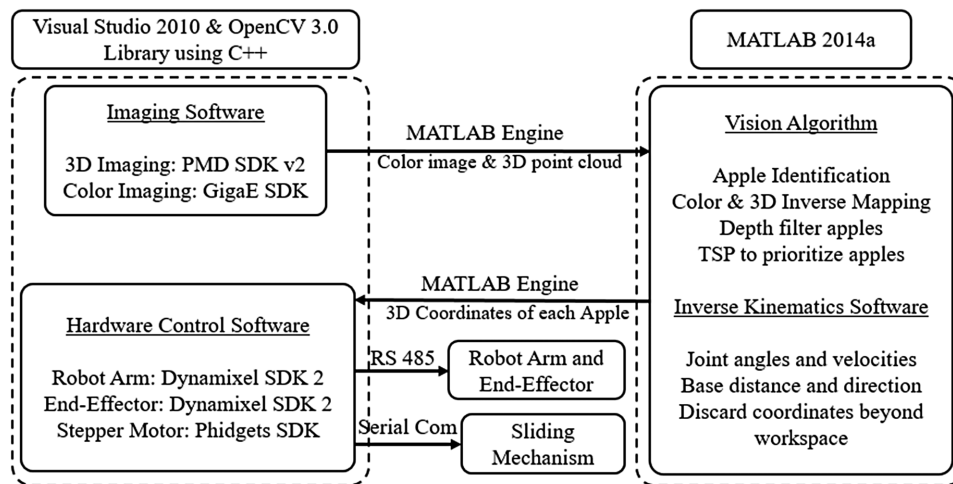


FIGURE 15 Software architecture showing individual programming procedure under C++ and MATLAB platform. The arrowheads indicate the direction of information flow using the MATLAB Engine



FIGURE 16 End-effector successfully grasping and rotating an apple



FIGURE 17 Picture of a picking failure. This apple was on a thin, flexible branch not secured to a trellis wire, so the branch was displaced along with the fruit. The apple was not separated or released and remained within the end-effector's grasp

Post inspection of the 127 fruit successfully harvested revealed no obvious evidence of bruising or surface damage. Because stem retention is desirable for fresh market apples, after each harvesting cycle all apples were inspected to determine whether the stem was intact (86/127), had pulled out of the stem cavity (8/127), or had the spur

TABLE 3 Comparison of average picking time, which measures physical manipulation during an apple pick, by cycle position

	Average Picking Time (s)	Standard Deviation (σ)
Overall	6.0	0.4
1 st apple in a cycle	6.2	0.6
Remaining apples in a cycle	5.8	0.4

attached (33/127). Earlier studies⁷⁴ on the importance of stem retention were not conclusive for all varieties, so this is a question that the research community and industry should review in more depth.

One of the major objectives of this research was to use well-defined performance criteria and segregate and report execution time of each major task individually. Figure 18 displays the contents of timing parameters for all major procedures. Vision timing included the sum of all listed procedures including apple identification, inverse mapping, and depth filtering. On average, 6.1 s was required to identify and localize all apples in an image, equivalent to 1.5 s of computation time per apple. IK time was measured as the time required to calculate joint velocities and angles for each path point for all apples as well as filter apples beyond the workspace. The mean computation time for path planning was 0.1 s per fruit. Picking time describes physical manipulation only and includes the time required to approach, grasp, remove, and drop an individual apple. The system's average picking time was 6.0 s. The total cycle time was the summation of vision processing, path planning computations, and manipulation of the fruit. Including the average vision time of 1.5 s, the total cycle time required to harvest a single apple was approximately 7.6 s. It should be noted that the cycle time reported here does not include the time required to reposition the vehicle between harvesting cycles. Because the largest movement was usually from the first apple in a cycle to the manipulator's waiting position, the average picking time for the first fruit was significantly higher than the remaining apples in a cycle. Table 3 compares the picking time of the first fruit in a cycle with the remaining fruit in that cycle.

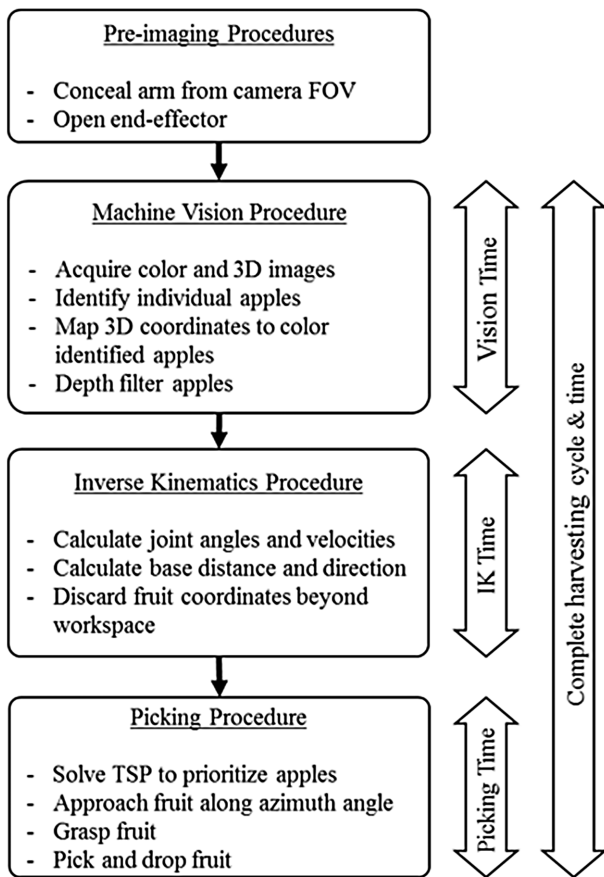


FIGURE 18 Time required to complete each procedure. Total cycle time includes vision processing, path planning computations, and physical manipulation of the fruit

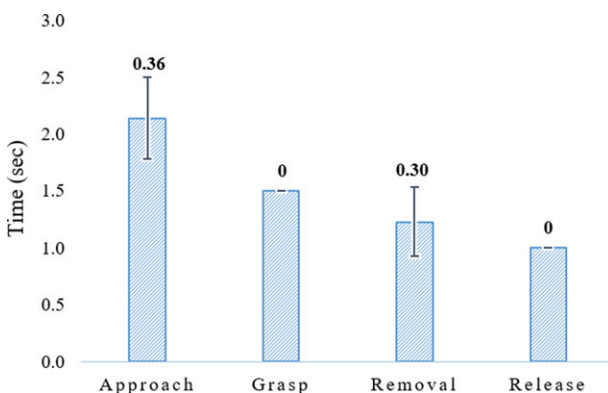


FIGURE 19 Average duration of each manipulation task. The standard deviation is reported with error bars

The duration of each manipulation subtask for every apple was also recorded. Approach to the fruit, grasping, removal, and release of the fruit (i.e., opening of the end-effector) were executed and timed as discrete software functions. The segregated breakdown of picking by timed task is shown in Figure 19. Grasping and release of the fruit were open-loop commands set at 1.5 s and 1.0 s, respectively. The approach, which includes the time after a fruit is released until the end-effector

reaches the next apple in a cycle, included the largest portion of average picking time at 36%.

11 | DISCUSSION

The goal of this research was to evaluate picking functionality using a low-cost robotic harvesting system. Excluding the electric utility vehicle, the total price for all mechanical manipulation hardware (e.g., actuators, electronics, etc.) was less than \$15,000 USD. The approach adopted was to assess performance in a modern orchard system with ideal fruit distribution. The key lessons learned from this research include the following themes

- A global camera set-up shows the potential to robustly detect and localize the apple center in 3D space. Additional imaging was not required between successive fruit picks. Exposure fusion enhanced vision performance by removing hard shadows and saturated regions of images acquired in the outdoor environment in bright daylight conditions. However, during field studies, calibration of hand-eye coordination was variable as the accuracy of the 3D camera slightly decreased when its internal temperature increased after several hours of operations (approximately 3 hours). Calibration changes could be the cause of some missed fruit. Further improvement in hand-eye calibration, including accounting for relative rotation in addition to translation, also needs to be considered.
 - The passive compliance incorporated in the end-effector design enhanced grasping robustness. As shown in Figure 20(a), the distal flexure was capable of deflecting during unplanned collisions without adverse effects. Likewise, Figure 20(b) shows the end-effector grasping a fruit in the presence of noticeable perception error. Both fruit picks shown in Figure 20 were successful. While the picking process did cause vibration of the tree and remaining fruit, vibration was sufficiently damped between each pick such that the end-effector could successfully grasp the next apple in the cycle. It is also important to note that the modular configuration of the end-effector helped reduce repair time. Only 10 min was required to remove and replace a finger mount in the field after it snapped when the end-effector unintentionally contacted a trellis wire while approaching a fruit.
 - Additional sensing is required for improved harvesting efficiencies and overall robustness. Previous studies of the force profile during the hand picking process²⁰ showed that the moment of fruit separation can be detected. Integrating force sensors in the end-effector is the subject of future work and will provide feedback about missed fruit and those not separated from the tree after the predetermined displacement. Also, during this research, the vision system identified only the fruit position. Preliminary studies have shown that robustly determining fruit orientation and stem location with the global camera system described in this paper is very challenging. Because of variability in growing orientation, implementing alternative fruit detachment methods that contact the stem may require visual detection/localization of the apple's stem.

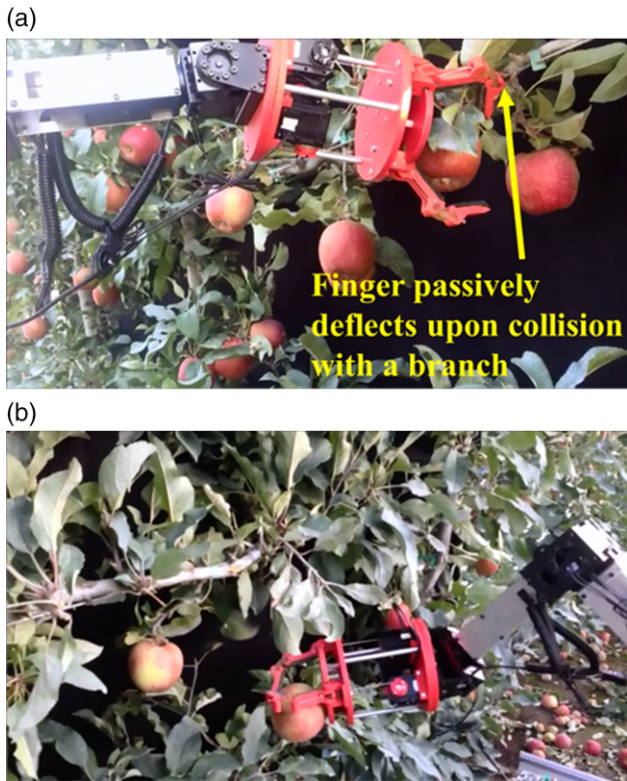


FIGURE 20 Advantages of passive compliance during apple picking. (a) A finger deflects during an unplanned collision with the main branch. (b) The end-effector completes a successful grasp in the presence of perception error

- It was learned that even with a planar canopy structure where access to individual fruit was better than traditional architectures, improved manipulation is required. More sophisticated manipulation, which depends on additional visual sensing of the environment, will improve system robustness. Workspace thinning was based on input from growers in Eastern Washington. For the implemented grasping strategy, 13% of the missed fruit were due to an end-effector finger making unplanned contact with an obstacle during grasping. With cluttered workspace conditions, a power grasp reliant on form closure of the apple is not robust for all fruit. Results of this work suggest that for a grasping end-effector, obstacle detection in conjunction with grasp planning has the potential to improve robustness. Likewise, obstacle detection may be required for expanding the system's workspace to additional regions of the canopy whereby harvesting will require multiple traverses of tree trunks and trellis wires. Implementation of vision algorithms for obstacle detection as well as motion planning fully exploiting kinematic redundancy for improved robustness is ongoing.
- Incorporating model-based design during the system design process should be a goal. As mentioned previously, the addition of the manipulator's seventh degree of freedom and corresponding modifications to the kinematics algorithm were relatively late design changes completed after lab tests and close to the start of the apple harvest. Hence, the resulting mechanical design of the prismatic base and iterative, numerical method used in the kinematics planner were not

optimized. Arikapudi et al.⁷⁵ have recently presented work on the digitization of orchard trees with the goal of developing design tools for simulation of virtual harvesting. Such efforts are critical for early design optimization as well as reducing the cost/time of the development cycle, especially in agricultural applications where the duration available for field studies is highly constrained.

- Horticultural practices are critical to the performance of robotic tree fruit harvesting systems. As described in Section 4, prior to harvesting, apples within 5 cm of a trunk/wire and directly behind the wire were removed from the workspace. Even under these ideal picking conditions, some of the remaining fruit proved problematic. Fruit that were in clusters of two to three and those that were on long, thin shoots were difficult to harvest. The ideal distribution of apples was individual fruit 5 to 15 cm away from rigid obstacles, such as trellis wires, sprinkler lines, and tree trunks, evenly distributed in the canopy on well-secured branches. The practice of pruning all leaves except those above the fruit is also advantageous.
- Finally, there are other practical considerations for commercial viability, especially weather proofing and fruit preparation for storage. During field studies, activities were significantly delayed by persistent fog because of concerns of moisture accumulation on electronic components. Additionally, high winds could move leaves and apples causing errors in both visual localization and manipulation. During field studies, small gusts of wind caused blurring of leaves in a few images with no apparent blurriness of the fruit. In our earlier work, we have also observed that during sunset and sunrise, the canopy was washed with access red light waves that altered the color saturation of the scene. This mainly affected the segmentation process and caused false positives in the fruit detection process. A supportive structure such as the over-the-row platform could help avoid these scenarios and provide protection against natural elements such as rain and the wind. However, compatibility of such structures with different types of modern orchard architectures (V-trellis, Y-trellis, Vertical trellis, etc.) should be considered. Also, for premium apple varieties with soft skins, like Honeycrisp and Fuji, workers clip the stems after detachment so that the stem does not puncture fruit in the bin used for field collection and storage. Considering this constraint, unless the clipping process is automated, varieties that do not require stem clipping prior to storage may be more suitable candidates for robotic harvesting.

12 | CONCLUSION

Robotic tree fruit harvesting is a difficult challenge, but there exists a clear need for the technology in today's economy. This paper presented the design and field testing of a robotic system designed to harvest fresh market apples. In order to assess required functionality in modern orchard systems with ideal fruit distributions, an undersensed, low-cost system was developed. Based on local growers' willingness to modify the tree to optimize fruit distribution for robotic harvesting, apples adjacent to trellis wires and trunks were removed prior to field studies. The robotic system integrated a global camera set-up, seven

DOF manipulator, and grasping end-effector to execute fruit picking with open-loop control. The system identified 100% of the apples with an average localization time of 1.5 s per fruit. Of the 150 fruit attempted, 127 were successfully detached from the tree with an average picking time of 6.0 s per fruit. Results from field studies show that horticultural practices play a critical role in the selection of functionality requirements. Improved harvesting efficiency will require enhanced robustness, especially obstacle detection with increased visual sensing and force sensing on the end-effector for feedback on grasp status.

ACKNOWLEDGMENTS

This research was supported in part by the United States Department of Agriculture (USDA)'s Hatch and Multistate Project Funds (Accession No 1005756 and 1001246), USDA National Institutes for Food and Agriculture competitive grant (Accession No 1000339), and Washington State University (WSU) Agricultural Research Center (ARC). Any opinions, findings, and conclusions expressed in this publication are those of the authors and do not necessarily reflect the view of the USDA or Washington State University. The authors would also like to acknowledge Allan Brothers Inc. and the Auvil Fruit Company for their support during field testing.

REFERENCES

- United States Department of Agriculture (USDA). Definition of specialty crops. Retrieved from <http://www.ams.usda.gov/AMSV1.0/scbgpdefinitions>. 2008.
- Washington State Employment Security Department. Agriculture workforce report. Retrieved from <https://fortress.wa.gov/esd/employmentdata/docs/industry-reports/agricultural-workforce-report-2013.pdf> (accessed April 27, 2016). 2013.
- Gallardo RK, Taylor M, Hinman H. 2009 cost estimates of establishing and producing 'Gala' apples in Washington. Washington State University Extension Factsheet FS005E. Pullman, WA: Washington State University; 2010.
- Fennimore SA, Doohan DJ. The challenges of specialty crop weed control. *Weed Technol.* 2008;22(2):364–372.
- Calvin L, Martin P. *The U.S. Produce Industry and Labor: Facing the Future in a Global Economy*. Economic Research Report No. 106. Economic Research Service, United States Department of Agriculture (USDA); 2010.
- Gonzalez-Barrera A. More Mexicans leaving than coming to the U.S. Pew Research Center. Retrieved from http://www.pewhispanic.org/files/2015/11/2015-11-19_mexican-immigration_FINAL.pdf (accessed November 24, 2015). 2015.
- Fathallah FA. Musculoskeletal disorders in labor-intensive agriculture. *Appl Ergonom.* 2010;41(6):738–743.
- Robinson T, Hoying S, Sazo MM, DeMarree A, Dominguez L. A vision for apple orchard systems of the future. *New York Fruit Q.* 2013;21(3):11–16.
- Gallardo RK, Brady MP. Adoption of labor-enhancing technologies by specialty crop producers: The case of the Washington apple industry. *Agric Finance Rev.* 2015;75(4):514–532.
- Elkins RB, Meyers JM, Duraj V, et al. Comparison of platform versus ladders for harvest in northern California pear orchard. *XI International Pear Symposium, ISHS Acta Horticulturae 909*. Patagonia, Argentina; 2011.
- Peterson DL, Bennedsen BS, Anger WC, Wolford SD. A systems approach to robotic bulk harvesting of apples. *Trans ASAE* 1999;42(4):871–876.
- Polat R, Gezer I, Guner M, Dursun E, Erdogan D, Bilim HC. Mechanical harvesting of pistachio nuts. *J Food Eng.* 2007;79(4):1131–1135.
- Torregrosa A, Orti E, Martin B, Gil J, Ortiz C. Mechanical harvesting of oranges and mandarins in Spain. *Biosystems Eng.* 2009;104(1):18–24.
- De Kleine ME, Karkee M. A semi-automated harvesting prototype for shaking fruit tree limbs. *Trans ASABE* 2015;58(6):1461–1470.
- Zhou J, He L, Karkee M, Zhang Q. Analysis of shaking-induced cherry fruit motion and damage. *Biosystems Eng.* 2016a;144:105–114.
- Zhou J, He L, Karkee M, Zhang Q. Effect of catching surface and tilt angle on bruise damage of sweet cherry due to mechanical impact. *Comput Electron Agric.* 2016b;121:282–289.
- Grand d'Esnon A, Pellenc R, Rabatel G, Journeau A, Aldon MJ. Magali: A self-propelled robot to pick apples. In: *ASAE Annual International Meeting*. Baltimore, MD; 1987.
- Harrell RC, Levi P. Vision controlled robots for automatic harvesting of citrus. In: *International Conference on Agricultural Engineering*, Paper No. 88.426. Paris, France; 1988.
- Bac CW, Van Henten EJ, Hemming J, Edan Y. Harvesting robots for high-value crops: state-of-the-art review and challenges ahead. *J Field Robot.* 2014;31(6):888–911.
- Davidson JR, Silwal A, Karkee M, Mo C, Zhang Q. Hand picking dynamic analysis for undersensed robotic apple harvesting. *Trans ASABE* 2016a;59(4):745–758.
- Sarig Y. Robotics of fruit harvesting: A state-of-the-art review. *J Agric Eng Res.* 1993;54(4):265–280.
- Burks T, Villegas F, Hannan M, et al. Engineering and horticultural aspects of robotic fruit harvesting: Opportunities and constraints. *HortTechnology* 2005;15(1):79–86.
- Li P, Lee S, Hsu H. Review of fruit harvesting method for potential use of automatic fruit harvesting systems. *Procedia Eng.* 2011;23:351–366.
- Gongal A, Amatya S, Karkee M, Zhang Q, Lewis K. Sensors and systems for fruit detection and localization: A review. *Comput Electron Agric.* 2015;116:8–19.
- Barnea E, Mairon R, Ben-Shahar O. Colour-agnostic shape-based 3D fruit detection for crop harvesting robots. *Biosystems Eng* 2016;146:57–70.
- Qiang L, Jianrong C, Bin L, Lie D, Yajing Z. Identification of fruit and branch in natural scenes for citrus harvesting robot using machine vision and support vector machine. *Int J Agric Biol Eng* 2014;7(2):115–121.
- Slaughter DC, Harrell RC. Discriminating fruit for robotic harvest using color in natural outdoor scenes. *Trans ASAE*. 1989;32(2):757–763.
- Bin L, Maohua W, Ning W. Development of a real-time fruit recognition system for pineapple harvesting robots. In: *ASABE Annual International Meeting*, Paper Number, 1009510. St Joseph, MI; 2010.
- Silwal A, Gongal A, Karkee M. Identification of red apples in field environment with over-the-row machine vision system. *Agric Eng Int.* 2014;16(4):66–75.
- Silwal A, Karkee M, Zhang Q. A hierarchical approach of apple identification for robotic harvesting. *Trans ASABE* 2015;59(5):1079–1086.
- Tabb AL, Peterson DL, Park J. Segmentation of Apple fruit from video via background modeling. In *2006 ASABE Annual International Meeting*. Portland, OR; 2006.
- Kurtulmus F, Lee WS, Vardar A. Green citrus detection using 'eigen-fruity', color and circular Gabor texture features under natural outdoor conditions. *Comput Electron Agric.* 2011;78(2):140–149.

33. Stajnko D, Rakun J, Blanke M. Modelling apple fruit yield using image analysis for fruit colour, shape and texture. *Eur J Horticultural Sci* 2009;74(6):260–267.
34. Ji W, Zhao D, Cheng F, Xu B, Zhang Y, Wang J. Automatic recognition vision system guided for apple harvesting robot. *Comput Electr Eng*. 2012;38(5):1186–1195.
35. Hannan MW, Burks TF. Current developments in automated citrus harvesting. In: ASAE/CSAE Annual International Meeting. Ontario, Canada; 2004.
36. Linker R, Cohen O, Naor A. Determination of the number of green apples in RGB images recorded in orchards. *Comput Electron Agric* 2012;81:45–57.
37. Plebe A, Grasso G. Localization of spherical fruits for robotic harvesting. *Machine Vision and Applications* 2001;13(2):70–79.
38. Zhao J, Tow J, Katupitiya J. On-tree fruit recognition using texture properties and color data. In *IEEE/RSJ International Conference on Intelligent Robots and Systems (IROS)*. Alberta, Canada; 2005.
39. Rakun J, Stajnko D, Zazula D. Detecting fruits in natural scenes by using spatial-frequency based texture analysis and multiview geometry. *Comput Electron Agric*. 2011;76(1):80–88.
40. Wang Q, Nuske S, Bergerman M, Singh S. Automated crop yield estimation for apple orchards. *Springer Tracts Adv Robot*. 2013;80:745–758.
41. Payne A, Walsh K, Subedi P, Jarvis D. Estimating mango crop yield using image analysis using fruit at 'stone hardening' stage and night time imaging. *Comput Electron Agric*. 2014;100:160–167.
42. Bulanon DM, Kataoka T, Okamoto H, Hata S. Determining the 3-D location of the apple fruit during harvest. In: *Automation Technology for Off-Road Equipment*. Kyoto, Japan; 2004.
43. Wachs JP, Stern HI, Burks T, Alchanatis V. Low and high-level visual feature-based apple detection from multi-modal images. *Precision Agric* 2010;11(6):717–735.
44. Wang J, Zhao D, Ji W, Tu J, Zhang Y. Application of support vector machine to apple recognition using in apple harvesting robot. *International Conference on Information and Automation (ICIA)*. Zhuhai/Macau, China; 2009.
45. Kong D, Zhao D, Zhang Y, Wang J, Zhang H. Research of apple harvesting robot based on least square support vector machine. In: *International Conference on Electrical and Control Engineering (ICECE)*. Zhenjiang, China; 2010.
46. Hung C, Underwood J, Nieto J, Sukkarieh S. A feature learning based approach for automated fruit yield estimation. *Springer Tracts Adv Robot*. 2015;105:485–498.
47. Baeten J, Donne K, Boedrij S, Beckers W, Claesen E. Autonomous fruit picking machine: A robotic apple harvester. *Springer Tracts Adv Robot*. 2008;42:531–539.
48. Bulanon DM, Kataoka T. Fruit detection system and an end effector for robotic harvesting of Fuji apples. *Agric Eng Int*. 2010;12(1):203–210.
49. Zhao D, Lu J, Ji W, Zhang Y, Chen Y. Design and control of an apple harvesting robot. *Biosystems Eng*. 2011;110(2):112–122.
50. Washington State Department of Agriculture. Washington tree fruit acreage report 2011. Retrieved from www.nass.usda.gov/Statistics_by_State/Washington/Publications/FruitTreeInventory2011.pdf (accessed April 27, 2015). 2011.
51. Bac CW, Hemming J, Van Henten EJ. Robust pixel-based classification of obstacles for robotic harvesting of sweet-pepper. *Comput Electron Agric*. 2013;96:148–162.
52. Font D, Palleja T, Tresanchez M, et al. A proposal for automatic fruit harvesting by combining a low cost stereovision camera and a robotic arm. *Sensors* 2014;14(7):11557–11579.
53. Mertens T, Kautz J, Van Reeth F. Exposure fusion: A simple and practical alternative to high dynamic range photography. In: *Computer Graphics Forum*. (vol. 28, No. 1, pp. 161–171). Blackwell Publishing Ltd; 2009.
54. Bouget JY. (2013). *Camera calibration toolbox for MATLAB*. Retrieved from http://www.vision.caltech.edu/bouguetj/calib_doc.
55. Van den Bergh M, Van Gool L. Combining RGB and ToF cameras for real-time 3D hand gesture interaction. In *IEEE Workshop on Applications of Computer Vision (WACV)*. Kona, HI; 2011.
56. Ringbeck T, Hagebeuker B. A 3D time of flight camera of object detection. Paper presented at the *Optical 3-D Measurement Techniques*. Switzerland: ETH Zurich; 2007.
57. Möller T, Kraft H, Frey J, Albrecht M, Lange R. Robust 3d measurement with pmd sensors. In: *Proceedings of the 1st Range Imaging Day*. Zürich, Switzerland; 2005.
58. Sivaraman B, Burks TF. Robot manipulator for citrus harvesting: Configuration selection. In *ASABE Annual International Meeting*. Minneapolis, MN; 2007.
59. Van Henten EJ, Van't Slot DA, Hol CWJ, Van Willigenburg LG. Optimal manipulator design for a cucumber harvesting robot. *Comput Electron Agric*. 2009;65(2):247–257.
60. Baur J, Pfaff J, Ulbrich H, Villgrattner T. Design and development of a redundant modular multipurpose agricultural manipulator. In: *IEEE/ASME International Conference on Advanced Intelligent Mechatronics*. Kaohsiung, Taiwan; 2012.
61. Lehnert C, Perez T, McCool C. Optimisation-based design of a manipulator for harvesting capsicum. In: *Workshop on Robotics in Agriculture at the International Conference on Robotics and Agriculture (ICRA)*. Seattle, WA; 2015.
62. Davidson JR, Silwal A, Hohimer CJ, Karkee M, Mo C, Zhang Q. Proof-of-concept of a robotic apple harvester. In: *IEEE/RSJ International Conference on Intelligent Robots and Systems (IROS)*. Daejon, Korea; 2016b.
63. Cutkosky MR. On grasp choice, grasp models, and the design of hands for manufacturing tasks. *IEEE Trans Robot Autom*. 1989;5(3):269–279.
64. Ma R. Yale OpenHand Project. Retrieved from <http://www.eng.yale.edu/grablab/openhand/>. 2014, September 1.
65. Odhner LU, Jentoft LP, Claffee MR, et al. A compliant, underactuated hand for robust manipulation. *Int J Robot Res*. 2014;33(5):736–752.
66. Dollar AM, Howe RD. The highly adaptive SDM hand: Design and performance evaluation. *Int J Robot Res*. 2010;29(5):585–597.
67. Davidson JR, Mo C. Mechanical design and initial performance testing of an apple-picking end-effector. In: *ASME International Mechanical Engineering Congress and Exposition (IMECE)*. Houston, TX; 2015.
68. Siciliano B. Kinematic control of redundant robot manipulators: A tutorial. *Journal of Intelligent and Robotic Systems* 1990;3(3):201–212.
69. Kizilateş G, Nuriyeva F. On the nearest neighbor algorithms for the traveling salesman problem. In: *Advances in Computational Science, Engineering and Information Technology*. Springer International Publishing; 2013:111–118.
70. Denavit J, Hartenberg RS. A kinematic notation for lower-pair mechanisms based on matrices. *Trans ASME J Appl Mech*. 1955;22:215–221.
71. Wang LT, Chen CC. A combined optimization method for solving the inverse kinematics problem of mechanical manipulators. *IEEE Trans Robot Autom*. 1991;7(4):489–499.
72. Luenberger DG, Ye Y. *Linear and Nonlinear Programming*. 3rd ed. New York: Springer; 2008.

73. Siciliano B, Sciavicco L, Villani L, Oriolo G. *Robotics Modelling, Planning and Control*. London: Springer; 2009.
74. Janisiewicz WJ, Peterson DL. Susceptibility of the stem pull area of mechanically harvested apples to blue mold decay and its control with a biocontrol agent. *Plant Disease* 2004;88(6):662–664.
75. Arikapudi R, Vougioukas S, Saracoglu T. Orchard tree digitization for structural-geometrical modeling. In: *Proceedings of the 10th European Conference on Precision Agriculture (ECPA)*. Israel: Volcani Center; 2015.

How to cite this article: Silwal A, Davidson JR, Karkee M, Mo C, Zhang Q, Lewis K. Design, integration, and field evaluation of a robotic apple harvester. *J Field Robotics*. 2017;34:1140–1159.
<https://doi.org/10.1002/rob.21715>